

Linear-Scaling Density-Functional Theory with Tens of Thousands of Atoms: Expanding the Scope and Scale of Calculations with ONETEP

Published as *Comput. Phys. Commun.* **180**, 1041 (2009)

N. D. M. Hine,¹ P. D. Haynes,¹ A. A. Mostofi,¹ C.-K. Skylaris² and M. C. Payne³

¹*Department of Physics and Department of Materials,*

Imperial College London, Exhibition Road, London SW7 2AZ, United Kingdom.

²*School of Chemistry, University of Southampton, Highfield, Southampton SO17 1BJ, UK and*

³*Theory of Condensed Matter group, Cavendish Laboratory,*

J J Thomson Avenue, Cambridge CB3 0HE, UK.

(Dated: March 31, 2011)

ONETEP is an *ab initio* electronic structure package for total energy calculations within density-functional theory. It combines ‘linear scaling’, in that the total computational effort scales only linearly with system size, with ‘plane-wave’ accuracy, in that the convergence of the total energy is systematically improvable in the manner typical of conventional plane-wave pseudopotential methods. We present recent progress on improving the performance, and thus in effect the feasible scope and scale, of calculations with ONETEP on parallel computers comprising large clusters of commodity servers. Our recent improvements make calculations of tens of thousands of atoms feasible, even on fewer than 100 cores. Efficient scaling with number of atoms and number of cores is demonstrated up to 32,768 atoms on 64 cores.

I. INTRODUCTION

Density-functional theory (DFT) is well-recognized as a versatile and powerful tool for studying condensed matter systems[1]. While it is now widely used for predicting static and dynamic properties of molecules and solids, it is similarly widely recognized that conventional DFT methods become severely inefficient at large system sizes. In the conventional Kohn-Sham approach, the computational effort involved in a total energy calculation scales asymptotically as the cube of the system size, restricting the approach to the study of no more than a few hundred atoms. However, for almost as long as this limitation has been known, a parallel methodological track has been developing: that of *linear scaling* DFT[2].

A number of codes now exist which implement variations on this linear scaling approach, using a number of different choices of basis set and approaches taken to the optimization of the energy or diagonalization of the Hamiltonian[3–8]. The code addressed in this paper, ONETEP, combines the benefits of linear scaling with a level of accuracy and variational bounds comparable to that of traditional cubic-scaling plane-wave approaches, often argued to be the most unbiased and controllably accurate method of performing a DFT calculation.

The formalism of linear scaling[9] is general for all systems with an energy gap, as this guarantees the exponential localization of the Wannier functions[10]. However, the demands of linear scaling vary considerably in different types of system, depending on the details of the periodicity, packing and electronic structure of the atoms involved. Most demonstrations of linear scaling DFT to date have focused on localized, finite systems or systems elongated in one or two dimensions, such as nanotubes, nanorods and slabs. Linear-scaling calcula-

tions in fully 3-dimensional-periodic systems, while possible within the framework, have remained challenging and time-consuming for reasons we will discuss. One useful measure of the value of a linear-scaling approach is known as the ‘crossover point’, and is defined as the number of atoms in the system at which the computational time for a total energy calculation becomes lower with a linear-scaling approach than with a traditional cubic-scaling approach of comparable accuracy. While it can be very low for isolated structures, this figure has remained high for fully-periodic solids treated with ONETEP, of the order of 300-500 atoms in favorable systems such as semiconductors, and up to 1000-1500 atoms in unfavourable systems such as metal oxides. To bring down this crossover, one must decrease the prefactor of the linear scaling by increasing the efficiency of the algorithms used.

ONETEP was developed from the beginning as a parallel code[11]. In this paper we will describe a number of improvements to the parallel algorithms of the ONETEP code, which have resulted in considerable speed-ups of almost all aspects of the package. Combined, these have enabled us to bring down the prefactor of linear scaling considerably for all systems. For solids, in particular, calculations which would have been unfeasibly slow can now be regarded as routine, and the true linear-scaling regime is fully accessible even to inexpensive clusters of commodity servers.

In Section II we will briefly outline the formalism used by ONETEP to achieve linear-scaling computational effort. We will then address some of the main challenges of practical implementation of this formalism and recent improvements in their scaling with system size and their efficiency on parallel computers, in Sections III, IV and V. Section III deals with the implementation of sparse matrix algebra and its varying performance in systems with

different sparsity characteristics. Section IV addresses the ‘row-sums’ operation common to many parts of the program, and Section V addresses successes in reducing and optimizing the use of Fourier transforms, which are in many cases the limiting factor on performance. Finally in Section VI we present benchmarks and demonstrations of linear scaling in various systems, over a wide range of sizes.

II. THEORETICAL BACKGROUND

Kohn-Sham DFT relies on the substitution of the real interacting system by a fictitious system of independent particles interacting with a mean-field potential $V[n](\mathbf{r})$, which is a functional of the density $n(\mathbf{r})$. The system is then described by the Hamiltonian

$$\hat{H}\psi_n(\mathbf{r}) = \left[-\frac{\hbar}{2m}\nabla^2 + V[n](\mathbf{r}) \right] \psi_i(\mathbf{r}) = \epsilon_i \psi_i(\mathbf{r}),$$

which must be solved self-consistently for the orthogonal single-particle states $\{\psi_i(\mathbf{r})\}$ with eigenvalues $\{\epsilon_i\}$. In a periodic system the orbitals are often labeled with a band index i and a \mathbf{k} -point \mathbf{k} , and known as Bloch orbitals. This system of noninteracting particles thus described can equivalently be fully described by the single-particle density matrix $\rho(\mathbf{r}, \mathbf{r}')$, which in terms of the Bloch states can be written as

$$\rho(\mathbf{r}, \mathbf{r}') = \sum_i \frac{V_{\text{cell}}}{(2\pi)^3} \int_{\text{BZ}} f_{i\mathbf{k}} \psi_{i\mathbf{k}}(\mathbf{r}) \psi_{i\mathbf{k}}^*(\mathbf{r}') d^3k.$$

The integral is over the 1st Brillouin Zone (BZ), and occupation numbers $f_{i\mathbf{k}}$ of 0 or 1 correspond to empty or filled states respectively. The charge density $n(\mathbf{r})$ is simply the diagonal part of the density matrix, $\rho(\mathbf{r}, \mathbf{r})$, multiplied by two if required to account for spin-degeneracy. Any approach which involves calculating and manipulating these Bloch functions directly will inevitably scale as $O(N^3)$: there must be at least $O(N)$ orbitals to describe the $O(N)$ electrons occupying them; each orbital extends over the whole system and thus any manipulation of it requires effort of $O(N)$; finally, the constraint of mutual orthogonality between these orbitals means that minimization of the energy can only be achieved with an extra $O(N)$ computational effort.

The steps that enable linear scaling are, firstly, to realize that the total energy can be calculated and minimized without ever explicitly calculating the energy eigenstates, and secondly that the density matrix is, in an insulator at least, ‘nearsighted’. The density matrix can always be represented in terms of a set of localized nonorthogonal functions $\{\phi_{\alpha\mathbf{R}}\}$, as

$$\rho(\mathbf{r}, \mathbf{r}') = \sum_{\alpha\beta} \sum_{\mathbf{R}} \phi_{\alpha\mathbf{R}}(\mathbf{r}) K^{\alpha\beta} \phi_{\beta\mathbf{R}}(\mathbf{r}'), \quad (1)$$

where we have also introduced the *density kernel* $K^{\alpha\beta}$ [12], representing a generalization of occupation numbers

to a nonorthogonal basis. The functions $\{\phi_{\alpha\mathbf{R}}\}$ are referred to as NGWFs (Nonorthogonal Generalized Wannier Functions) [13], and can be thought of as a combination of a subspace rotation $\mathbf{M}(\mathbf{k})$ of the Bloch orbitals at each \mathbf{k} and a unitary transformation in \mathbf{k} -space, localizing them to a supercell at position \mathbf{R} :

$$\phi_{\alpha\mathbf{R}}(\mathbf{r}) = \frac{V}{(2\pi)^3} \int_{\text{BZ}} e^{-i\mathbf{k}\cdot\mathbf{R}} \left[\sum_i \psi_{i\mathbf{k}}(\mathbf{r}) M_{i\alpha}(\mathbf{k}) \right] d\mathbf{k}.$$

Within ONETEP, these functions are expressed in terms of a basis of periodic bandwidth-limited delta functions, or psinc functions [13, 14], and are strictly localized to a spherical region of radius R_{ϕ_α} . These psinc functions, with coefficients $C_{i,\alpha}$, are centered on the grid points \mathbf{r}_i of a regular grid, the spacing of which is determined by a plane-wave cutoff energy E_{cut} with a similar meaning to that in a plane-wave code.

Given a set of NGWFs $\{\phi_\alpha\}$ in the home simulation cell (such that $\mathbf{R} = 0$) and a density kernel $\{K^{\alpha\beta}\}$, one can calculate the Kohn-Sham total energy, expressed as

$$E[\{K^{\alpha\beta}\}, \{\phi_\alpha\}] = K^{\alpha\beta} H_{\beta\alpha} + E_{\text{DC}}[n], \quad (2)$$

where the first term is the bandstructure energy and E_{DC} compensates for the double-counting of density interactions present in the first term. A summation is implied over repeated Greek indices throughout. The matrix elements of the Hamiltonian are constructed for each pair of overlapping NGWFs by techniques which achieve linear scaling with system size by means of the so-called ‘FFT box’ technique described previously [15]. In this approach, the psinc functions are projected into a box of fixed size, generally smaller than the simulation cell, which is then used for all Fourier transforms required to calculate the parts of the Hamiltonian which are more easily treated in reciprocal space.

To find the ground state energy of a given system, one must minimize Eq. 2 simultaneously with respect to the density kernel elements $K^{\alpha\beta}$ and the coefficients describing the NGWFs themselves. ONETEP achieves this optimization by means of two nested loops: the outer loop optimises the basis set by minimizing the interacting energy with respect to the NGWF coefficients, while the inner loop optimises the density kernel by minimizing the energy for a given set of NGWFs with respect to the density kernel elements. We express the outer loop as

$$E_{\text{min}} = \min_{\{C_{i,\alpha}\}} L(\{C_{i,\alpha}\}), \quad (3)$$

where the coefficients $C_{i,\alpha}$ are nonzero only for psinc functions i at points \mathbf{r}_i within the localization radius of ϕ_α . The inner loop, performed at fixed $C_{i,\alpha}$, minimizes the energy with respect to the kernel elements $K^{\alpha\beta}$

$$L(\{C_{i,\alpha}\}) = \min_{\{K^{\alpha\beta}\}} E(\{K^{\alpha\beta}\}; \{C_{i,\alpha}\}). \quad (4)$$

This minimization ensures that in Eq. 3, L is a function only of the coefficients $C_{i,\alpha}$.

The technical details of the implementation of this scheme have been described in some detail elsewhere[8, 11, 13–18]. In this article, we will discuss only the aspects of the scheme underlying the time-limiting steps of this calculation. By maximizing the efficiency of these steps through consideration of the properties of typical physical systems, it is possible to extend the scope and scale of linear-scaling plane-wave DFT calculations to unprecedented heights.

III. SPARSE MATRIX ALGEBRA

Achieving true linear scaling of computational effort relies on the fact that the density kernel, expressed as a matrix in terms of the NGWFs in Eq. 1, is ‘nearsighted’. This means that the scale of matrix elements between distant NGWFs decays exponentially with the separation of the centers of these NGWFs: $K^{\alpha\beta}$ can then be truncated for NGWF centers separated by more than some cutoff length, when $|\mathbf{R}_\alpha - \mathbf{R}_\beta| > R_K$. This ensures \mathbf{K} has a high degree of sparsity in the limit of large systems, as each NGWF ϕ_α has nonzero density kernel elements $K^{\alpha\beta}$ only with a system-size-independent number of other nearby NGWFs ϕ_β . For a suitably chosen ordering of the atoms (achieved in ONETEP by means of a Peano space-filling curve[19]), the nonzero elements of \mathbf{K} are clustered near the diagonal of the matrix. For a set of strictly localized functions ϕ_α of range R_ϕ the overlap \mathbf{S} and Hamiltonian \mathbf{H} will also be short-ranged and thus sparse. Algebraic manipulation of these sparse matrices can therefore in principle be achieved in $O(N)$ time given sufficient sparsity.

It is therefore crucial to the implementation of linear-scaling methods to have a sparse matrix algebra methodology capable of dealing efficiently with the multiplication of matrices whose sparsity pattern corresponds to that of typical real systems of atoms. Previous descriptions of the parallel algorithms of ONETEP have focused on the efficient parallel evaluation of operator integrals, and the sparse algebra routines have not previously been described: here we will briefly introduce the parallel sparse matrix algebra routines, and focus on how they have been optimised for efficient scaling.

All the matrices considered here are of size $N \times N$ where N is the number of NGWFs required to represent the occupied orbitals of the atoms present. This can exceed 10^5 in the largest calculations presented in this work. The elements of the matrix must therefore be distributed over the parallel nodes of the computer running the simulation. The atoms are distributed over the nodes, and the data corresponding to columns of the sparse matrix are stored only on the node to which the atom of each column belongs. The sparse indexing is dealt with by ‘atom-blocking’, where a block corresponding to the atom in column i and row j is of size $m_i \times m_j$, where m_i is the number of NGWFs on atom i . This means that rather than recording the NGWF rows for which each col-

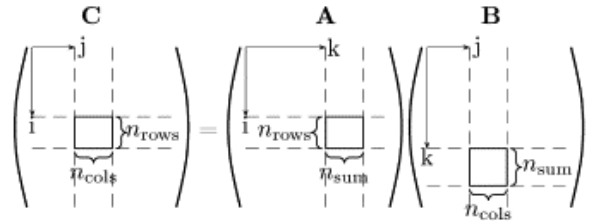


Figure 1: Schematic representation of the multiplication of one pair of blocks during a sparse matrix multiplication in ONETEP. On the left is matrix \mathbf{C} , the block shown of which contains a contribution from the blocks of \mathbf{A} and \mathbf{B} , on the right. The dimensions of the blocks guarantee compatibility of the matrix sizes. Efficiency of these small block matrix-multiplication operations is crucial to the overall speed of the matrix algebra.

umn is nonzero, we can record the atom block-rows for which each atom block-column is nonzero. This works because all the NGWFs for a species of atom have the same radius, so if any NGWF on a particular atom overlaps with one on another atom, they all do. Within the block, the data for each NGWF column is stored sequentially, and the computational overhead of indexing and cache-latency of sparse algebra is thus greatly reduced.

However, despite this efficient design, the performance of the sparse algebra routines has, in previous implementations of the method, been one of the main limiting factors on the speed of calculations, preventing efficient operation beyond a few thousand atoms. A first, relatively trivial step to improving this performance was to optimize the innermost loop of the sparse product by considering the physical systems to which it will most often be applied. Consider the operation $C^{\alpha\beta} = A^{\alpha\gamma} B_{\gamma\beta}$, where \mathbf{A} , \mathbf{B} and \mathbf{C} are sparse matrices which may have different sparsity patterns. Figure 1 shows this multiplication schematically. To perform the product, three nested loops are required: first, over the block-columns j of \mathbf{B} and \mathbf{C} , parallelised over the nodes over which the atoms are distributed; second over all the nonzero block-rows k of \mathbf{B} ; and finally, for each block found, over the block-rows i which are nonzero in both \mathbf{A} and \mathbf{C} . If the data for the required block-column of \mathbf{A} is not local to the node on which the contribution from a particular column of \mathbf{B} is being evaluated, it must be communicated to this node. There is therefore an outermost loop over the other nodes and, for each step, the nodes receive data from a different other node. Since each individual NGWF sphere only overlaps a system-size-independent number of its neighbours, there are only $O(1)$ nonzero row elements in each column. This means that in principle the operation can be completed in $O(N)$ operations overall.

For one node-node pair, the pairs of blocks of \mathbf{A} and \mathbf{B} thus identified as contributing to \mathbf{C} are matrix-multiplied together and added to those of \mathbf{C} . The fact that each matrix obeys the same blocking scheme means that the number of rows n_{rows} in the block of \mathbf{C} is the same as in \mathbf{A} , the number of columns n_{cols} in the block of \mathbf{C} is the same as

Abbrev.	System	$E_{\text{cut}} / \text{eV}$	R_K / a_0	R_ϕ / a_0	N_{at}	N_ϕ	N_{iter}
C960	(12,0) Carbon Nanotube	400	20	6.7	960	3840	4
BgK Toxin	Organic Anemone Toxin	500	22	6.0	581	1466	10
Alumina331	α -Alumina $3 \times 3 \times 1$ cell	1200	24	7.7	270	1080	1
GaAs rod	Wurtzite GaAs Nanorod	400	40	10.0	430	1222	4
Silicon444	Silicon $4 \times 4 \times 4$ cell	600	20	7.2	512	2048	1

Table I: Key to the abbreviations used for the 5 different systems used for performance testing. Systems were chosen to represent a cross-section of common uses of ONETEP (nanostructures, organic molecules, semiconductor and oxide solids, etc) and different extremes of cutoff energy E_{cut} and kernel and NGWF cutoffs R_K and R_ϕ . The number of atoms N_{at} and NGWFs N_ϕ are also shown. The numbers of iterations N_{iter} were chosen so as to keep the total times for each system comparable.

in \mathbf{B} , and the number of columns n_{sum} in the block of \mathbf{A} is the same as the number of rows in the block of \mathbf{B} . We therefore have three numbers n_{rows} , n_{cols} and n_{sum} describing the block-multiply. In principle, these can have any value, but some physical insight into the systems being simulated allows considerable speedup. Because the NGWFs in a particular atom-block represent an *in situ* optimized basis for that atom, one need only ever put enough NGWFs on each atom to represent the occupied pseudo-atomic orbitals, taking into account the symmetry properties required due to their being centered on the atoms. For example, if only the uppermost *s*- and *p*-bands are occupied, 4 NGWFs are sufficient (1 to represent the *s* orbital and 3 for the p_x , p_y and p_z orbitals). The overwhelming majority of block sizes in a real calculation are therefore in the set $\{1, 4, 5, 9, 10\}$, depending on the species of atom and the nature of the bonding. By hard-coding the matrix multiplication for many of the combinations of these commonly occurring values, we avoid the overhead of library calls for these trivial matrix-multiplications.

The result, for simulations where the multiplication operations for the required block sizes are hard-coded, is a dramatic decrease in the total time taken for sparse algebra operations. A rough guide is a factor of 10 when executed on a single processor, though the specific value depends on the library call being compared against. However, this speedup in the time for the actual mathematical operation brings into clearer focus two further issues: firstly, that the communications patterns can be improved greatly by physical considerations of the optimal distribution of atoms over nodes for a realistic system, and secondly, that in many typical systems, the matrices being calculated are not, in comparatively small systems, of a great enough size that sparse algebra is actually worthwhile at the typical filling fractions that occur. Figure 2 shows a comparison of the time taken for 10 sparse matrix products when using generic matrix multiplication code, versus the time for the loop-unrolled version of the inner loop of the block multiplication. The range of systems tested is meant as a cross section of typical uses of the code demonstrating different challenges in different parts of the code, and is explained in Table I.

Building on this success, we can obtain further system-

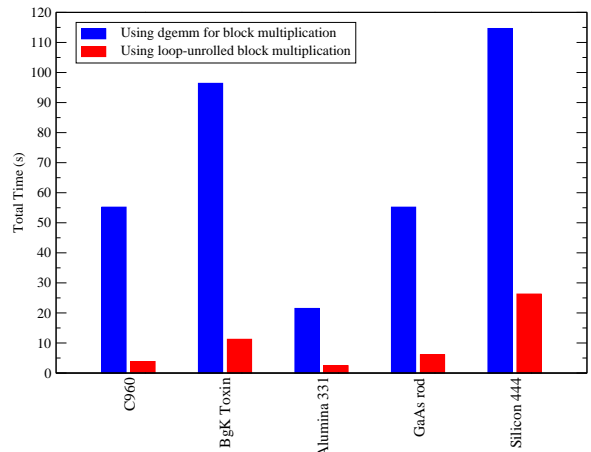


Figure 2: (color online) Total time for 10 sparse matrix product operations on 4 cores of a dual-socket, dual-core Intel Woodcrest node. We compare the operation using the LAPACK routine ‘dgemm’ to the same operation with all the block multiplication operations unrolled for efficient vector operation. Table I shows a key to the abbreviations labelling the systems.

dependent speedup by analysing the properties of the dominant sparse algebra on which the main optimization cycle of the code relies, so as to alleviate the limiting factors on performance. ONETEP uses two approaches to the optimization of the density kernel: the penalty functional approach of Haynes and Payne[18] and our own modification of the Li, Nunes, Vanderbilt [20–22] variational approach. The latter is in use during the main loop of the program. In this approach, one defines the following electronic Lagrangian:

$$L(\mathbf{K}) = E(\tilde{\mathbf{K}}) - \mu(2\text{Tr}[\tilde{\mathbf{K}}\mathbf{S}] - N_e),$$

where $\tilde{\mathbf{K}}$ is the McWeeny purified density kernel[12],

$$\tilde{\mathbf{K}} = 3\mathbf{K}\mathbf{S}\mathbf{K} - 2\mathbf{K}\mathbf{S}\mathbf{K}\mathbf{S}\mathbf{K}, \quad (5)$$

and $E(\tilde{\mathbf{K}})$ is the total energy functional of this purified kernel. Inspection of Eq. 5 shows that if there is to be no truncation during the intermediate steps of updating the kernel, one must deal with matrices whose degrees

of sparsity are very much lower than that of the kernel itself. For example, the least sparse matrix one calculates before the result is truncated has the form $(\mathbf{KSKS})^{\alpha}_{\beta}$, and this can be nonzero for any $\phi_{\alpha}, \phi_{\beta}$ pair separated by a distance $|\mathbf{R}_{\alpha} - \mathbf{R}_{\beta}|$ of up to $2R_{\mathbf{K}} + 4R_{\phi}$. This very greatly reduces the sparsity of the resulting matrix, compared to that of the kernel itself. Furthermore, it is often desirable to be able to carry out calculations with no kernel truncation, and not just in metals where the kernel cannot be truncated for physical reasons. Even though linear scaling will not be obtained in very large systems, below a threshold of a few thousand atoms the computational time taken performing matrix algebra is negligible compared to other parts of the calculation.

Sparse matrix multiplication is only a benefit compared to simply padding a full-square matrix with zeros as long as the overhead of sparse indexing is lower than the time saved by avoiding the unnecessary multiplication of zero elements. In practice, this means that sparse matrices are not worth using unless they are around 90% sparse or more. It is therefore often possible to obtain a time saving by neglecting the sparse matrix indexing and simply using a fully dense form for small systems. We have therefore implemented an option within ONETEP to activate dense matrix algebra in place of the sparse matrices.

Comparisons of the performance of the two approaches can be seen in Figures 3 and 4. Here we consider a typical sparse matrix product of a type which occurs many times per iteration. Denoting the sparsity pattern of the density kernel by K and the sparsity pattern of the overlap matrix by S, here we show an operation where the sparsity patterns of the matrices in the product are $\text{KS} \times \text{K} \rightarrow \text{KSK}$. For a typical solid, diamond-structure silicon, with $R_{\phi} = 6.8a_0$ for the NGWFs and $R_{\mathbf{K}} = 24a_0$ for the density kernel, we consider supercells of $N_{\text{at}} = 8M^3$ atoms, resulting from repeating the 8-atom simple cubic unit cell M times in each direction. The degree of sparsity of these matrices as a function of the number of atoms in the supercell is shown in Table II. Figure 3 shows the timings for 10 repetitions of a matrix product between the two with both approaches. We vary both N_{at} and the number of CPU cores N_P to show the scaling with the size the system and the number of cores used for the calculation. Figure 4 shows the timings for the matrix trace of a product of the same two matrices, which does not require evaluation of the full matrix product and thus scales differently with N_{at} and N_P .

The conclusion is as one would expect: dense matrix algebra is considerably faster at low filling fractions but scales as a much worse power of N : $O(N_{\text{at}}^3)$ for matrix multiplication, and $O(N_{\text{at}}^2)$ for the trace of a matrix product. With sparse algebra, the operations respectively scale as $O(N_{\text{at}}^3)$ and $O(N_{\text{at}}^2)$ initially, while the filling fraction is still high, but both become $O(N_{\text{at}})$ above a certain system size, once the system already contains all the atoms within range of the various cutoffs. This occurs at around $N_{\text{at}} = 1000$ in the system shown here —

Table II: Filling fractions of matrices of different sparsity patterns for cubic supercells of fcc silicon. K is the sparsity pattern of the density kernel, which is cutoff at $R_{\mathbf{K}} = 24a_0$, and S is the sparsity pattern of the overlap matrix, which is generated from the overlap of NGWFs of radius $R_{\phi} = 6.7a_0$. KS is the sparsity patterns of a matrix product of the kernel and overlap matrix, and KSK is the sparsity pattern of the product of this matrix with the kernel again.

N_{at}	S	K	KS	KSK
64	93.75%	100.00%	100.00%	100.00%
216	40.28%	100.00%	100.00%	100.00%
512	16.99%	78.52%	100.00%	100.00%
1000	8.70%	44.10%	98.10%	100.00%
1728	5.03%	25.52%	77.78%	100.00%
2744	3.17%	16.07%	54.34%	100.00%
4096	1.73%	10.77%	35.23%	98.19%
8000	0.89%	5.51%	18.04%	73.15%

beyond this point a graph of $T(N_{\text{at}})/N_{\text{at}}$ would be seen to be flat as a function of N_{at} . Sparse algebra takes over as the faster method once we pass $N_{\text{at}} = 1728$. At this point, the kernel sparsity is 75% and the overlap sparsity is 95%, but the KS structure is still only 22% sparse and KSK is still at 0% sparsity. As one would expect from the algorithm described above, it is clear that the sparsity of the multiplier and the multiplicand are more significant than that of the product in determining the time for the operation. These results appear to be typical for solids, though of course the rate at which the filling fraction changes with N_{at} depends on the values chosen for $R_{\mathbf{K}}$ and R_{ϕ} and the crystal structure of the solid. The choices of localization radii used here correspond to a simulation able to match with a high degree of accuracy the results of a plane wave calculation of equivalent cutoff energy[23].

It is crucial that a linear-scaling DFT code scales efficiently to very large numbers of processors, as it is only in large systems that the benefits of the formalism will be obtained. Concurrent with the aforementioned improvements to the algorithms for the matrix algebra, and advantageous to its performance in both sparse and dense formats, we have implemented a new communications pattern for the sparse algebra routines. The importance of the communications pattern can be seen by considering the occupation of a typical matrix where the nonzero elements are determined by the overlaps of spheres centered on atoms ordered by a space-filling curve. Figure 5 shows a typical sparsity pattern for the overlap matrix in a block of the silicon system considered above. It can be seen that the space-filling curve is fairly successful in clustering the nonzero elements of the matrix onto the diagonal even in a solid.

The consequence of this clustering is that the load balance must be carefully considered when performing matrix multiplication. The atoms, and thus the matrix data,

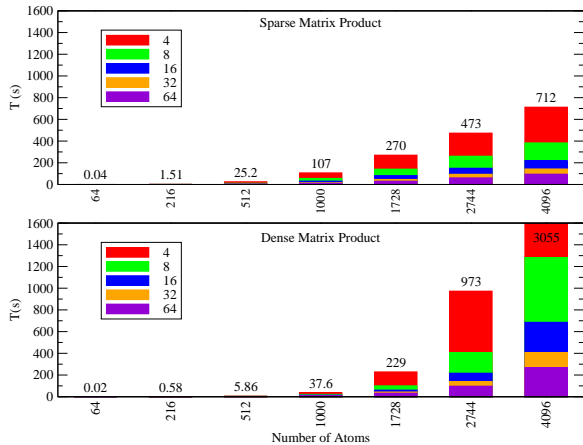


Figure 3: (color online) Total time for 10 matrix product operations for matrices of typical sparsity levels for a solid, parallelized over varying numbers of cores. The overlaid colored bars represent different numbers of cores. The dimension of the matrix is $4N_{\text{at}}$ as there are 4 NGWFs per atom. Above: Block-indexed sparse matrices. Below: Fully dense matrices. Sparse algebra becomes linear-scaling with N_{at} above a threshold of around 1000 atoms, whereas dense algebra remains $O(N^3)$. Sparse algebra therefore becomes faster somewhere around 2000 atoms. As the number of processors scales up, the total time scales down by nearly the same amount — the slight decrease from full $1/N_P$ scaling of total time being due to the extra communication overhead at higher N_P . As N_{at} increases, the maximum efficient value of N_P increases with it.

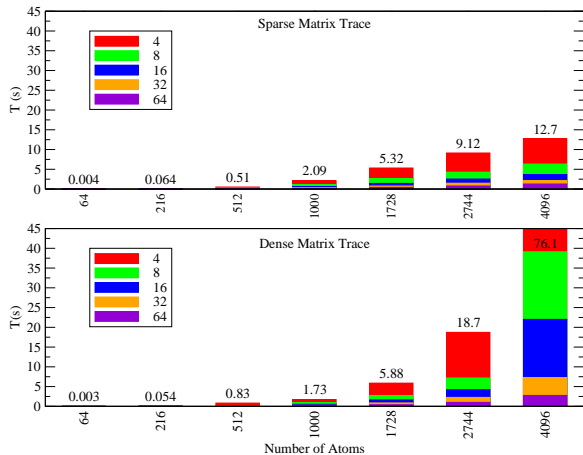


Figure 4: (color online) Total time for 10 matrix trace operations for the product of two matrices of typical sparsity levels for a solid. Above: Block-indexed sparse matrices. Below: Fully dense matrices.

are distributed over the nodes of the parallel computer: All nodes must in general communicate with all other nodes in order to perform a matrix multiplication, so the operation is divided into N_p node-steps. However, there are multiple options for the ordering of the communication and calculation. If the communications pattern is such that at node-step m all nodes work simultane-

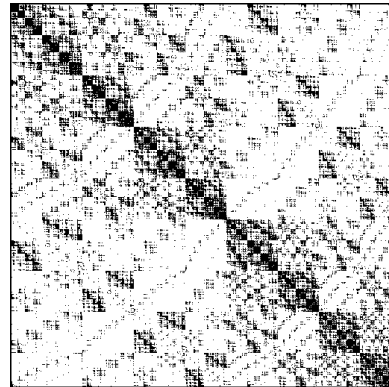


Figure 5: Sparsity pattern of the overlap matrix of a 512-atom block of solid silicon ($M = 4$). Blocks shown in black represent atoms whose radius $6.7a_0$ spheres overlap. The atoms have been ordered according to a Peano space-filling curve, which has the effect of grouping together nearby atoms, such that the nonzero elements cluster on the diagonal.

ously on the portion of node m 's data that overlaps their segment of the matrix, the load for that node-step will be very unevenly balanced, since clearly node m will take very much longer on that node-step than any other node. We therefore order the communication so that each node first works on its own data, then steps off the diagonal by one to work on the next node's data (modulo N_p), then the next, and so forth. In this manner, each individual node-step is approximately the same length on each processor.

Figure 6 compares the time taken for 10 sparse matrix multiplication operations with varying numbers of atoms on a 64 node cluster. With the old communications pattern, in which a 'blocking' communications operation (`mpi_bcast`) was used to communicate the data stored on each node to all other nodes at each step, sparse algebra performance was becoming severely limited by 64 nodes and large numbers of atoms. With the new system, the communications algorithm improvements have resulted in more than a 50% speedup (over and above any speedup due to improved block multiplication or dense matrix algebra).

As a result of considerable development work on the sparse algebra routines therefore, motivated by considerations of the physical system being studied, the sparse algebra performance of ONETEP has been sped up by a very considerable factor. On a small number of nodes this factor is around 10. However, the speedup scales with number of cores due to the removal of 'blocking' communications operations: on 64 cores, a factor of 20 or more can be obtained relative to the original implementation.

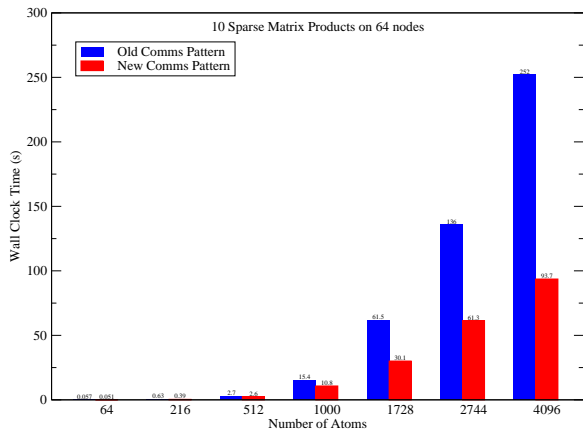


Figure 6: (color online) Comparison of old and new communications patterns. Left bars: Blocking communications routines. Right bars: Diagonal-patterned nonblocking, communications routines. The performance gain achieved by this physically-motivated reorganization increases with the number of nodes N_P . Already at 64 nodes the new approach is more than twice as fast as with the blocking routines.

IV. NGWF-NGWF PAIR OPERATIONS

One of the main challenges of linear-scaling DFT is the evaluation of the entire Hamiltonian matrix with algorithms that scale as $O(N)$, in that each element of the Hamiltonian matrix is evaluated with a computational effort that does not increase with the size of the system beyond a certain point. This is achieved in ONETEP by the use of the FFT box approach[15, 16]. Several of the routines in ONETEP which employ the FFT box approach share many elements of their algorithmic structure, the common element of which we will describe as ‘row sums’. Considerable reduction in the prefactor of linear scaling can be obtained by exploiting this similarity, which is the result of the common spatial localization of the NGWFs, to optimize the improve the performance of the algorithms used to evaluate various quantities.

The common structure of these routines can be seen by examining the intermediates we must evaluate in order to calculate the following: i) the kinetic energy E_{kin} via the kinetic matrix $T_{\alpha\beta}$, ii) the local potential (sum of the Hartree and XC potentials and the local part of the pseudopotential) via the local potential matrix $V_{\alpha\beta}^{\text{loc}}$, iii) the density $n(\mathbf{r})$, and iv) a precursor to the NGWF gradient. Expressions for these are given below:

- i) $E_{\text{kin}} = K^{\alpha\beta} \langle \phi_\alpha | \hat{T} | \phi_\beta \rangle$
- ii) $E_{\text{loc}} = K^{\alpha\beta} \langle \phi_\alpha | V_{\text{loc}} | \phi_\beta \rangle$,
- iii) $n(\mathbf{r}) = K^{\alpha\beta} \phi_\alpha(\mathbf{r}) \phi_\beta(\mathbf{r})$,
- iv) $\partial E / \partial \phi_\alpha(\mathbf{r}) = Q^{\alpha\beta} \phi_\beta(\mathbf{r}) + \dots$

for some matrix $Q^{\alpha\beta}$ with the sparsity pattern of $K^{\alpha\beta}$. In each case, the kernel (or other matrix of the same spar-

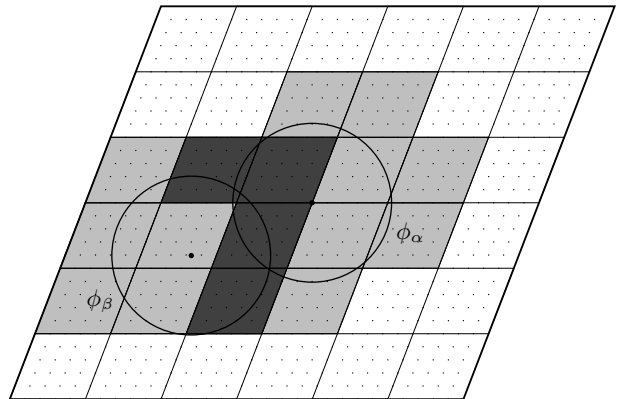


Figure 7: Schematic 2D slice of an FFT box cut out of a rhombohedral unit cell, centered on ϕ_α . Parallelepiped domains (ppds) within the sphere of ϕ_α or ϕ_β only are shown in light gray, and ppds within the spheres of both ϕ_α and ϕ_β in dark gray. Calculations such as overlaps need only consider the ppds common to both spheres. For matrix elements such as $\langle \phi_\beta | \nabla^2 | \phi_\alpha \rangle$, calculation of $\nabla^2 \phi_\alpha(\mathbf{r})$ via a Fourier transform delocalizes it over the whole FFT box. However, one can still save computation by extracting the result to the ppds of ϕ_β summing the overlap only over these points, as elsewhere ϕ_β is zero.

ity) is multiplying what is effectively a matrix of overlaps or products of functions, and the distribution of NGWFs over nodes means that each node only needs to calculate those elements of this matrix where ϕ_α belongs to that node. For each ϕ_α , therefore, there are some number of NGWFs ϕ_β for which some operation must be performed: for the kinetic energy, this is the Laplacian followed by calculation of the overlap with ϕ_α , for the density, it is Fourier interpolation with ϕ_β and deposition to the accumulating FFT box, and so on. A full description of this system can be found in Figures 2-5 of Reference [11] and the accompanying text, so we only summarize it here.

The ϕ_β functions that overlap with each ϕ_α will not necessarily be local to the node of ϕ_α , so some communication of NGWFs is required. These NGWFs are stored in a so-called ‘ppd representation’ (see Reference [11]), where their values are recorded on the points inside a number of parallelepipeds (ppds) which are regions of the full simulation cell determined by division of the full grid in to parallelepiped-shaped regions of fixed numbers of points along each axis. Figure 7 shows a schematic representation of the benefits of the ppd approach.

Communication of NGWF values between processors is performed by sending lists of the ppds within the NGWF sphere, and the psinc coefficients on the points in those ppds. For large radius spheres, this communication can take of order hundreds of microseconds, and there may be many millions of NGWF pairs to calculate per node. Additionally, because it is often not feasible to store the FFT boxes of every NGWF on each node simultaneously, a batch system is implemented so as to work on a batch of columns at a time. A loop runs over batches of as many NGWFs as fit in memory, and having received each

ϕ_β , it is applied to every ϕ_α in the batch with which it overlaps. However, if an NGWF ϕ_β overlaps multiple ϕ_α functions in different batches, it must be recomunicated several times. Furthermore, the time taken to perform the inner operation (overlap or product) on each NGWF is small but not negligible, and serves to exacerbate any inefficiencies in the communications caused by any degree of serialization. It is therefore of great importance to optimize the pattern of communication within a batch so as to maximize performance.

The communication pattern implemented prior to the current version is described in detail in Reference [8]. Briefly, this consisted of a double loop, first over node-node blocks of the matrix starting with the diagonal, then over NGWF pairs for that block, all in synchrony between nodes. To avoid otherwise catastrophic serialization where columns have overlaps that need calculating only on a small number of processors at a time, the outer loop was performed in two stages. First, the node-node blocks on or below the diagonal were processed, eliminating one node-column from the calculation after each off-diagonal row. Second, the blocks above the diagonal were dealt with, again eliminating one node-column each time but in the reverse order to during the first stage, giving $2N_P - 1$ steps in total. This ensured that the communication overlapped calculation efficiently in as much as the limiting case was the calculations being performed on the first node during the first stage, and the last node during the second stage. However, in both stages, all the nodes could often actually only be performing computation (rather than just waiting to send NGWFs) on average a little over half the time. Communications therefore accounted for upwards of 50% of the time during this stage of the calculation, and could be considerably worse in the case of densely overlapping solids, where the large number of NGWFs required by the first node from the last node tended to overflow available MPI buffers and cause considerable further slowdown.

For the new approach, we note that it is a relatively simple task to prepare a list of the row-column pairs that need calculating on each node for a particular batch of columns using the sparse matrix index. By calculating this ‘plan’ and sharing it with all the nodes before calculating the overlaps or products, an optimized communications pattern is automatically available to each node. The maximum number of overlaps or products on any node is the number of ‘plan steps’ n_p . A loop over this number of plan steps occurs on each processor, and for each step the node first examines the plan of every other node to determine whether it is required to send a new NGWF to that node. It then examines its own plan to determine whether it is going to receive a new NGWF from any node. Having done so (or loaded the NGWF into a buffer in the case where the plan calls for a local NGWF on that step), it proceeds to calculate the overlap for that row-column pair (or add the row function to an accumulating FFT box for that column in the case of products). In practice, the sending of the NGWFs can

pre-empt the corresponding receipt, simply by looking ahead in the plan by a set number of steps to determine what to send.

Further speedups can be obtained by cache-optimization of the operation itself. In the case of the routines involving the overlap of a function represented by the grid point values on the ppds of a sphere with the grid point values of a function in an FFT box, we have removed all instances where the ppd was deposited to full 3D boxes. Instead, given that the values of the first function is only nonzero on the ppd points, the values of the second function can be extracted to the ppds of the sphere of the first function. Then, by multiplying the ppd values together as a column vector, the overlap is obtained with far fewer operations. This speeds up the calculation of the local potential and kinetic matrices considerably. A similar procedure works to speed up the density and NGWF gradient ‘row sums’ $\sum_{\beta \cap \alpha} \phi_\beta(\mathbf{r})$. Because the multiplication of $\phi_\alpha(\mathbf{r})$ and $\phi_\beta(\mathbf{r})$ must be performed on the fine grid to avoid errors due to aliasing, one must deposit the values of $\phi_\beta(\mathbf{r})$ to an FFT box, in order to use Fourier interpolation. By streamlining this process into a straightforward ppd-by-ppd deposition of values rather than an extraction to a minimal box followed by a deposition of this box to the FFT box, the use of intermediate arrays has been removed. This results in a speedup of more than a factor of two in cases where this memory transfer was occurring outside of cache due to the size of the FFT box.

Figures 8-10 show the effect of these changes on the time taken to perform the parts of the calculation that can be limited by row sums. Figure 8 shows the time taken for a full calculation of the density across various systems, which are varyingly more or less dominated by the batch row sums part. Figures 9 and 10 show the times for calculation of the local potential and kinetic matrices respectively. All of these show significant improvements, particularly the density evaluation.

V. OPTIMIZATION OF NGWF GRADIENT AND FOURIER TRANSFORMS

The outer loop of the calculation is the minimization of the total energy with respect to the NGWF coefficients — effectively an optimization of the minimal basis set. To minimize the energy accurately with respect to these coefficients one must be able to calculate both the functional and the gradient of the functional with respect to the coefficients. The main computational effort of this optimization is divided into two parts: minimizing the electronic Lagrangian using the LNV approach (the inner loop), and calculation of the energy gradient in the space of NGWF psinc function coefficients (the ‘NGWF gradient’). The full expression for the NGWF gradient varies according to the scheme being used, but for the psinc coefficient of a particular NGWF ϕ_α corresponding

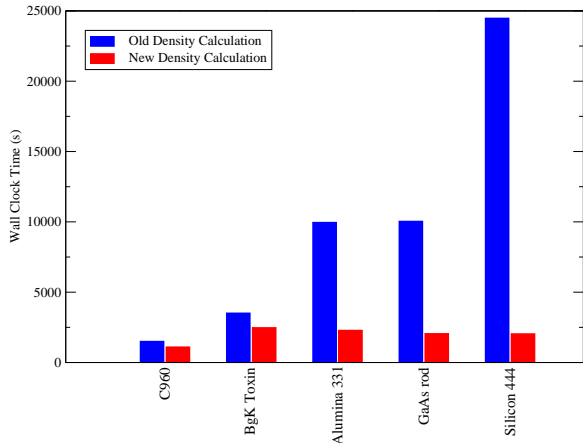


Figure 8: (color online) Comparison of ‘planned’ and ‘unplanned’ communications patterns during the calculation of the density, plus modifications to deposition of functions to FFT boxes. Calculations performed on 4 dual-socket, dual-core nodes (16 cores) of Imperial’s CX1 machine (Intel Woodcrest CPUs). Left bars: Old system. Right bars: new system. All the systems show considerable improvement, the more so the more their NGWFs overlap. Crystalline solids show a particularly large speed-up, since they necessarily have a large number of densely overlapping NGWFs. Table I shows a key to the abbreviations labelling the systems.

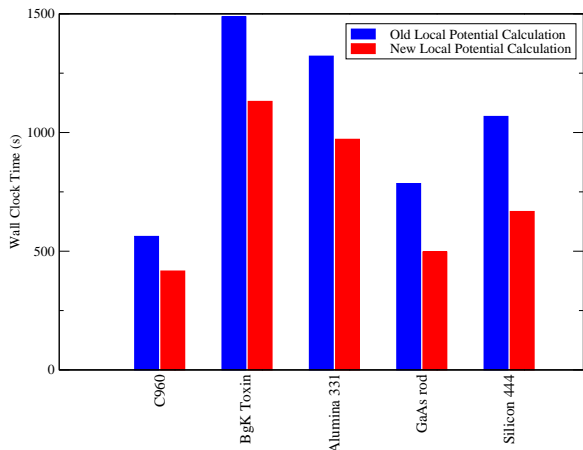


Figure 9: (color online) Comparison of ‘planned’ and ‘unplanned’ communications patterns during the calculation of the local potential matrix, combined with the effect of calculating of overlap integrals by extracting the functions from FFT boxes to ppds. Left bars: Old system. Right bars: new system.

to the point at \mathbf{r}_i , it always takes the general form

$$\frac{\delta E}{\delta C_{i,\alpha}} = \sum_{\beta} [\hat{H}\phi_{\beta}](\mathbf{r}_i) A_{\alpha}^{\beta} + \sum_{\gamma} \phi_{\gamma}(\mathbf{r}_i) B_{\alpha}^{\gamma},$$

for some choice of matrices A_{α}^{β} and B_{α}^{γ} . In Section IV we detailed improvements to the row sums, which is used for the latter expression, but this is often only a minor part of this calculation. Considerably more demanding,

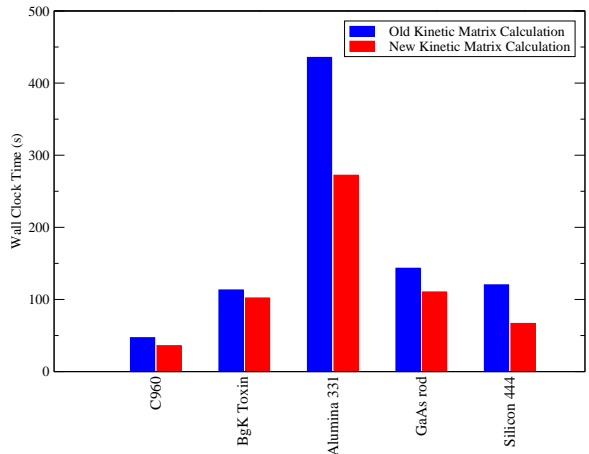


Figure 10: (color online) Comparison of ‘planned’ and ‘unplanned’ communications patterns during the calculation of the kinetic matrix, combined with the effect of calculating of overlap integrals by extracting the functions from FFT boxes to ppds. Left bars: Old system. Right bars: new system. Those systems where the FFT time dominates over the communications and ‘row sums’ part have not improved significantly. However, those with densely overlapping long ranged NGWFs, particularly the crystalline solid systems still show an improvement.

usually, is the calculation of the first part — the Hamiltonian acting on the NGWFs.

In the Hamiltonian, we can combine the Hartree $V_H(\mathbf{r})$ and exchange-correlation $V_{xc}(\mathbf{r})$ terms (calculated directly from the density) with the local pseudopotential $V_{ps,loc}(\mathbf{r})$ to form a total local potential $V_{loc}(\mathbf{r})$. We then need to consider only three separate terms: kinetic energy, local potential, and nonlocal pseudopotential. We are therefore calculating, on the grid points inside the localization radius of each ϕ_{α} , the following expression

$$\begin{aligned} \sum_{\beta\Gamma\alpha} [\hat{H}\phi_{\beta}](\mathbf{r}) &= -\frac{1}{2}\nabla^2 \sum_{\beta\Gamma\alpha} K^{\alpha\beta} \phi_{\beta}(\mathbf{r}) \\ &+ V_{loc}(\mathbf{r}) \sum_{\beta\Gamma\alpha} K^{\alpha\beta} \phi_{\beta}(\mathbf{r}) \\ &+ \sum_{\beta\Gamma\alpha} \sum_{\mu\Gamma\beta} \frac{K^{\alpha\beta} \langle P^{\mu} | \phi_{\beta} \rangle}{D_{\mu}} P^{\mu}(\mathbf{r}) \end{aligned}$$

where P^{μ} are the nonlocal projectors and D_{μ} the corresponding Kleinman-Bylander denominators, labeled by an index μ which runs over the projectors for each angular momentum state on each atom with nonlocal channels in its pseudopotential.

A batch system has previously been partially implemented for this part of the calculation, but only for the local potential extraction part. One batch of accumulating FFT boxes contains the ‘row sums’ $\sum_{\beta} K^{\alpha\beta} \phi_{\beta}(\mathbf{r})$ on the points in the FFT box centered on ϕ_{α} , with the sum over β including all the NGWFs ϕ_{β} overlapping ϕ_{α} . The local potential $V_{loc}(\mathbf{r})$ in the region for which ϕ_{α} is

nonzero must be extracted from the distributed, whole-cell array in which it is stored. One can therefore save on repeated extraction of the local potential if the FFT box containing ϕ_α has not moved from one NGWF in the batch to the next (as will often occur since there are multiple NGWFs on each atom).

This batch system has now been extended to cover the nonlocal potential part of the calculation. Previously, for each ϕ_α , there was a loop over the projectors overlapping all the ϕ_β functions overlapping ϕ_α . If a projector contributed to the sum, it was generated from its reciprocal space radial representation once per NGWF ϕ_α . However, since there are multiple NGWFs on each atom requiring the same projector at the same position in their FFT box, the batch system allows us to calculate these projectors only once per batch. This represents a very considerable saving on time spent Fourier transforming and shifting the projector functions.

To avoid errors due to aliasing, the calculation of local potential contribution is performed by multiplying the FFT box and the local potential together on the fine grid (which has twice the spacing of the standard grid). This routine has been improved considerably by improvements to the Fourier interpolation routines. By careful consideration of cache efficiency, and by avoiding unnecessary repeated normalizations, the routines have been uniformly sped up by around 40%.

Figure 11 shows the combined effects of these improvements. The total time for calculation of the NGWF gradient is shown for the same set of different systems as the previous figures. In this case it is the GaAs nanorod, with its large radius NGWFs, and hence large FFT boxes, that takes longest — and also shows the greatest speedup as the overhead of recreating projectors is removed.

VI. RESULTS

In the preceding sections, we have detailed changes to the ONETEP code designed to improve the absolute speed of the code and its scaling with both system size and number of processors. We will now examine the overall effects of these changes. Most significant is the improvement in sparse algebra, which, in systems where this was the limiting factor (generally speaking, anything both well into the linear-scaling regime and larger than around 4000 atoms), has improved in performance by a factor of at least 5-10, and more on larger numbers of cores. Second, in solid systems, where row sums performance was limiting on large numbers of nodes, the optimization of these routines has resulted in a factor of 5-10 (more system dependent) speedup in these areas of the code. Considerable work has also gone in to optimizing the initialization routines. Previously these contained many $O(N^2)$ steps that took negligible time and were thus judged not to matter as they were only performed once per calculation, such as initialisation of the ppd lists describing each sphere. However, as the system

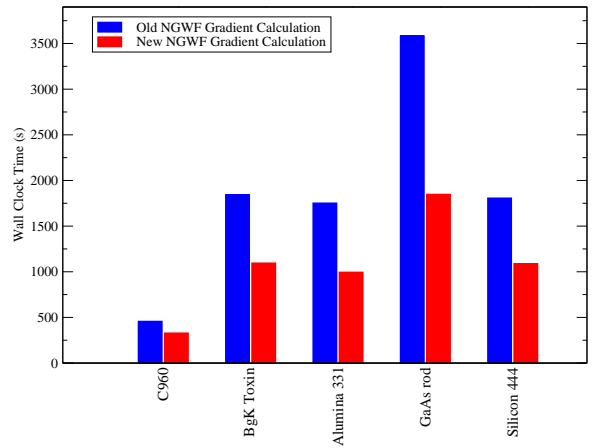


Figure 11: (color online) Comparison of old and new systems for the calculation of NGWF gradients. Improvements include the ‘planned sums’ system for calculating the accumulating FFT boxes $\sum_\beta \phi_\beta(\mathbf{r})$, the saving of repeated calculations of identical projectors, and improvements in Fourier interpolation and Fourier filtering. Considerable speedup has been obtained across all systems — again, particularly those with densely overlapping NGWFs. Left bars: Old system. Right bars: new system.

size grows these inevitably grow to become comparable to the $O(N)$ steps. However, most have now been replaced by alternative algorithms which have only $O(N)$ scaling, greatly reducing the the initialization time. The only remaining algorithms scaling worse than $O(N)$ are the Ewald sum (which is rarely a significant contribution to the total time) and the initialization of the whole-cell structure factor for each species, which is $O(N^2)$. There are methods available to improve the scaling of Ewald sums to $O(N^{1.5})$ or better [24], and in even larger systems Fast Multipole Methods [25] may be the answer to calculating these long range electrostatic interactions in $O(N)$ but at present the system sizes involved are not large enough to necessitate their use. Overall, for a full single-point energy calculation for a system size over a few thousand atoms and on a few tens of cores or more, the new code (version 2.2.12) is typically a factor of between 3 and 10 times faster than the previous most recently-reported version (version 2.0.1).

Figure 12 shows the total time for one full iteration of the code on cubic supercells of fcc silicon of increasing size. Full comparison against previous versions of the code would be unfeasible for the systems shown here, due to the amount of wall clock time required even for a single iteration of the old version at the larger system sizes. The results display near-perfect linear scaling of the total time per iteration at system sizes up to 32,768 atoms. The only limitation preventing larger systems from being tested on this hardware was the memory per core, which was nearly full by 32,768 atoms on 64 cores at this cutoff energy. Spreading the calculation over 256 cores or more would enable a 100,000 atom equivalent calculation. The

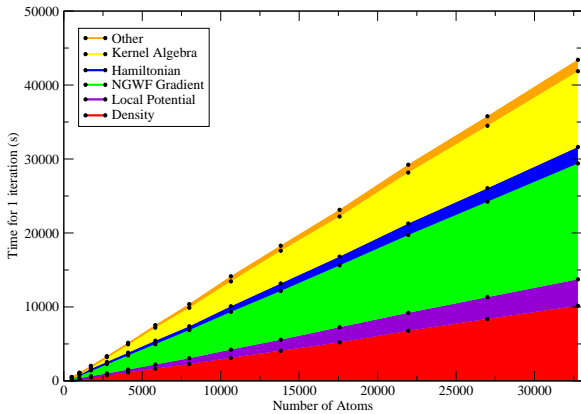


Figure 12: (color online) Timings for one iteration of ONETEP 2.2.12 on 64 cores (16 dual-socket, dual-core nodes) of Imperial’s CX1 cluster, calculating the total energy of a supercell of diamond structure silicon of increasing size. The total compute time is broken down by color into the various tasks performed each iteration. The dominant tasks are the calculation of the electron density (red), matrix algebra during kernel optimization (yellow), and calculation of the NGWF coefficient gradient (green). This calculation converges in around 12-15 iterations, independent of system size.

number of NGWF iterations required for convergence remains roughly constant with system size, not exceeding around 12-14, due to the efficient preconditioning of the gradient [14].

In Figure 13, we show the total times for the range of systems presented above (note the varying number of iterations between different systems, chosen to keep the total time approximately equal for easier comparison). Considerable improvements have been obtained across the range of systems, up to as much as an order of magnitude. Combined with the improved scaling with number of cores, this represents a very large increase in the feasible scale of problems that can be tackled with this approach. The sparse algebra improvements are at their most significant in systems previously dominated by sparse algebra time, such as the 960-atom segment of carbon nanotube, so this shows the greatest improvement of all the systems. However, it is the speedup of the densely overlapping systems such as the 3x3x1 Alumina supercell (120 atoms) which is most significant in terms of extending the range of applicability of ONETEP. Previously, it would not have been feasible on medium-sized clusters to access the linear scaling regime, the onset of which in a system with such large NGWFs is upwards of 1000 atoms since the number of points in an FFT box continues to grow as $O(N^3)$ up to this point. With the six- to ten-fold increase in performance of the row sums routines, such calculations are now routine on clusters of 16 or more cores.

The prevailing trend in high performance computing is towards ever larger clusters of high-performance, high-memory nodes composed of standard server CPUs connected with high-performance interconnects such as In-

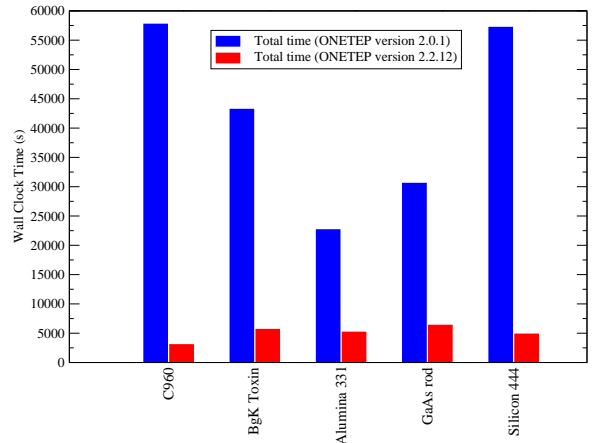


Figure 13: (color online). Total timings on 4 dual-socket, dual-core nodes (16 cores) for the most recent version of the code, 2.2.12, compared against those for version 2.0.1, which was current at the time of previous reports (eg Reference [23]). Table I shows a key to the abbreviations labelling the systems.

finiband. Consequently, it is important to know how a code scales to such large clusters. Previous results have demonstrated scaling of ONETEP from 1 to ~ 100 cores, and shown near-perfect parallelization, in that the wall clock time falls as nearly $1/N_P$ with increasing number of cores. However, as one improves the serial performance of the code so that the parallel overheads become more significant, and as one goes to larger numbers of cores, it becomes harder to maintain this scaling. This is true of many applications: for example, a common way of using traditional plane wave codes to simulate non-periodic systems is to perform calculations on a large supercell at the Gamma-point only. One does not then benefit from the parallelization of k -points over nodes, and while performance gains from parallelizing the code over G -vectors are rapid at small numbers of cores, communications overheads come to dominate over around 100 cores and minimal further improvement is obtained.

In ONETEP, communications overheads are very much less, as they are only a serious issue within the sparse algebra routines. In Figure 14 we present results obtained on a large cluster consisting of AMD Opteron dual-core nodes, the EPCC’s HECToR machine. We show the speedup relative to the time for the calculation on 64 nodes on 64, 128, 192 and 256 cores. There remains considerable improvement to be obtained even up to 256 cores, which is nearly a factor of 3 faster than with 64 cores, but clearly the improvement is beginning to saturate due to communications overheads. A fit to Amdahl’s law[26] (which predicts the maximum speedup possible for an algorithm of which only a fraction P can be parallelized) fits the data well. At larger system sizes or with larger cutoffs this saturation point will come at a higher number of cores. Additionally, compared to a traditional plane-wave calculation at the gamma point (i.e. not benefitting from k -point parallelization), Figure 14

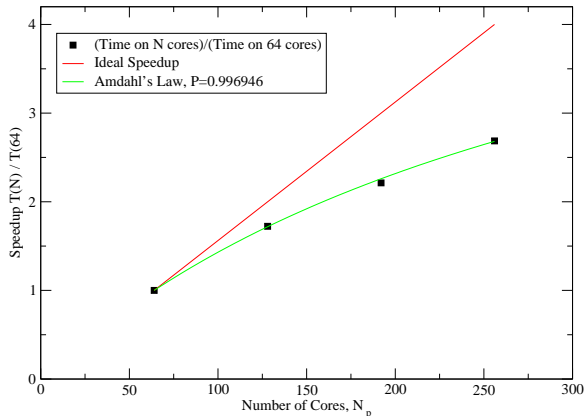


Figure 14: (color online) Parallel scaling for one iteration of the 27,000 atom silicon system from Figure 12, on 64 to 256 cores of HECToR. The ‘speedup’ is normalized to be equal to 1 at 64 cores (the smallest number on which this calculation fits in memory). Also shown is the ideal speedup ($N_P/64$) and a fit to Amdahl’s Law[26], which estimates the parallel fraction $P = 0.9969$.

represents very much more favourable improvement with system size. It is worth noting that, with the exception of the sparse algebra routines, all other parts of the calculation scale almost perfectly as $1/N_p$. Further work on the parallel scaling of the sparse algebra routines is expected to improve this performance.

VII. CONCLUSION

We have presented a combination of improvements to the ONETEP code obtained by consideration of the fac-

tors limiting performance in typical systems. Sparse matrix algebra performance has been sped up by the largest factor, but there are also very notable improvements to the performance of many of the other tasks the code performs.

The scaling with the number of cores has been improved considerably. Previous results had shown this to be nearly linear in ideal systems such as nanotubes, but in solids performance became limited by communications inefficiencies at large system sizes. Now, with much more efficient parallel algorithms, use of the code in solids of thousands or tens of thousands of atoms has been demonstrated to be fast and efficient.

Acknowledgments

One the authors (N.D.M.H.) acknowledge the support of the Engineering and Physical Sciences Research Council for postdoctoral funding (EPSRC Grant No. EP/F010974/1, part of the HPC Software Development program). P.D.H. and C.-K.S. acknowledge the support of University Research Fellowships from the Royal Society. A.A.M. acknowledges the support of the RCUK fellowship program.

Of great importance to this work was access to the computing resources of Imperial College’s High Performance Computing service (CX1), which has enabled most of the results presented here. Additionally, for the ability to perform larger calculations we acknowledge the computing resources provided by the EPSRC on the HECToR machine of the Edinburgh Parallel Computing Centre (EPCC).

-
- [1] M. C. Payne, M. P. Teter, D. C. Allan, T. A. Arias and J. D. Joannopoulos, *Rev. Mod. Phys.* **64**, 1045 (1992).
 - [2] S. Goedecker, *Rev. Mod. Phys.* **71**, 1085 (1999) .
 - [3] J. M. Soler, E. Artacho, J. D. Gale, A. García, J. Junquera, P. Ordejón and D. Sánchez-Portal, *J. Phys.: Condens. Matter* **14**, 2745-2779 (2002).
 - [4] D. R. Bowler, R. Choudhury, M. J. Gillan, T. Miyazaki, *phys. stat. sol. (b)* **243**, 989 (2006).
 - [5] J. VandeVondele, M. Krack, F. Mohammed, M. Parrinello, T. Chassaing and J. Hutter, *Comp. Phys. Commun.* **167** (2005).
 - [6] J.-L. Fattebert and J. Bernholc, *Phys. Rev. B* **62**, 1713 (2000); J.-L. Fattebert and F. Gygi, *Phys. Rev. B* **73**, 115124 (2006).
 - [7] M. Challacombe, *J. Chem. Phys.* **110**, 2332 (1999)
 - [8] C.-K. Skylaris, P. D. Haynes, A. A. Mostofi and M. C. Payne, *J. Chem. Phys.* **122**, 084119 (2005).
 - [9] G. Galli, M. Parrinello, *Phys. Rev. Lett.* **69** (1992) 3547.
 - [10] C. Brouder, G. Panati, M. Calandra, C. Mourougane, and N. Marzari, *Phys. Rev. Lett.* **98**, 046402 (2007).
 - [11] C.-K. Skylaris, P. D. Haynes, A. A. Mostofi and M. C. Payne, *phys. stat. sol. (b)* **243**, 973 (2006).
 - [12] R. McWeeny, *Rev. Mod. Phys.* **32**, 335 (1960).
 - [13] C.-K. Skylaris, A. A. Mostofi, P. D. Haynes, O. Diéguez and M. C. Payne, *Phys. Rev. B* **66**, 035119 (2002).
 - [14] A. A. Mostofi, P. D. Haynes, C.-K. Skylaris and M. C. Payne, *J. Chem. Phys.* **119**, 8842 (2003).
 - [15] C.-K. Skylaris, A. A. Mostofi, P. D. Haynes, C. J. Pickard and M. C. Payne, *Comput. Phys. Commun.* **140**, 315 (2001).
 - [16] A. A. Mostofi, C.-K. Skylaris, P. D. Haynes and M. C. Payne, *Comput. Phys. Commun.* **147**, 788-802 (2002).
 - [17] C.-K. Skylaris, P. D. Haynes, A. A. Mostofi and M. C. Payne, *J. Phys.: Condens. Matter* **17**, 5757 (2005).
 - [18] P. D. Haynes and M. C. Payne, *Phys. Rev. B* **59**, 12173 (1999) .
 - [19] M. Challacombe, *Comput. Phys. Commun.* **128**, 93 (2000).
 - [20] X.-P. Li, R. W. Nunes and D. Vanderbilt, *Phys. Rev. B* **47**, 10891 (1993).
 - [21] M. S. Daw, *Phys. Rev. B* **47**, 10898 (1993).
 - [22] P. D. Haynes, C.-K. Skylaris, A. A. Mostofi and M. C.

- Payne, *J. Phys.: Condens. Matter* **20**, 294207 (2008).
- [23] C.-K. Skylaris and P. D. Haynes, *J. Chem. Phys.* **127**, 164712 (2007).
- [24] J. Perram, H. Petersen and S. DeLeeuw, *Mol. Phys.* **65**, 875 (1988).
- [25] L. Greengard, V. Rokhlin, *J. Comput. Phys.* **73**, 325 (1987) .
- [26] G. Amdahl, *AFIPS Conference Proceedings*, **30**, 483 (1967).